



香港城市大學
City University of Hong Kong

專業 創新 胸懷全球
Professional · Creative
For The World

CityU Scholars

Heat Transfer Enhancement of n-Type Organic Semiconductors by an Insulator Blend Approach

Zhang, Zhuoqiong; Tang, Yabing; Wang, Yunfan; Zeng, Zixin; Shi, Run; Yan, Han; Tsang, Sai-Wing; Cheng, Chun; So, Shu Kong

Published in:
ACS Applied Materials and Interfaces

Published: 06/07/2022

Document Version:
Final Published version, also known as Publisher's PDF, Publisher's Final version or Version of Record

License:
CC BY

Publication record in CityU Scholars:
[Go to record](#)

Published version (DOI):
[10.1021/acsami.2c05503](https://doi.org/10.1021/acsami.2c05503)

Publication details:
Zhang, Z., Tang, Y., Wang, Y., Zeng, Z., Shi, R., Yan, H., Tsang, S.-W., Cheng, C., & So, S. K. (2022). Heat Transfer Enhancement of n-Type Organic Semiconductors by an Insulator Blend Approach. *ACS Applied Materials and Interfaces*, 14(26), 30174–30181. <https://doi.org/10.1021/acsami.2c05503>

Citing this paper

Please note that where the full-text provided on CityU Scholars is the Post-print version (also known as Accepted Author Manuscript, Peer-reviewed or Author Final version), it may differ from the Final Published version. When citing, ensure that you check and use the publisher's definitive version for pagination and other details.

General rights

Copyright for the publications made accessible via the CityU Scholars portal is retained by the author(s) and/or other copyright owners and it is a condition of accessing these publications that users recognise and abide by the legal requirements associated with these rights. Users may not further distribute the material or use it for any profit-making activity or commercial gain.

Publisher permission

Permission for previously published items are in accordance with publisher's copyright policies sourced from the SHERPA RoMEO database. Links to full text versions (either Published or Post-print) are only available if corresponding publishers allow open access.

Take down policy

Contact lbscholars@cityu.edu.hk if you believe that this document breaches copyright and provide us with details. We will remove access to the work immediately and investigate your claim.

Heat Transfer Enhancement of n-Type Organic Semiconductors by an Insulator Blend Approach

Zhuoqiong Zhang, Yabing Tang, Yunfan Wang, Zixin Zeng, Run Shi, Han Yan, Sai-Wing Tsang, Chun Cheng,* and Shu Kong So*



Cite This: *ACS Appl. Mater. Interfaces* 2022, 14, 30174–30181



Read Online

ACCESS |



Metrics & More



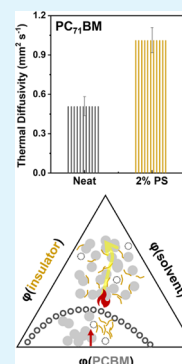
Article Recommendations



Supporting Information

ABSTRACT: The transfer of heat energy in organic semiconductors (OSCs) plays an important role in advancing the applications of organic electronics, especially for lifetime issues. However, compared with crystalline inorganic semiconductors, the thermal transport of OSCs is less efficient and a relevant understanding is very limited. In this contribution, we show that the heat conduction of OSCs can be enhanced by blending with a “commodity” insulator (both thermal and electrical). PC₇₁BM, a well-known electron transporter but poor thermal conductor, was selected as the host OSC material. The blending of a small amount of polystyrene (PS), a commonly used insulating polymer, can facilitate the heat transfer of PC₇₁BM films, as substantiated by the scanning photothermal deflection technique and an infrared thermal camera. The phase thermodynamics of PC₇₁BM/PS blends indicates that the efficient heat transfer preferably occurs in the OSC/insulator blends with better intimate mixing, where isolated PC₇₁BM domains can be effectively bridged by PS that thread through the regions. The applicability of this approach can be observed in blends with another host material—ITIC. This work provides a facile strategy for designing thermally durable organic electronic devices.

KEYWORDS: insulator blends, thermal stability, heat transfer, thermal transport, thermal management, organic field-effect transistor, n-type organic semiconductors



1. INTRODUCTION

Organic semiconductors (OSCs) possess many attractive attributes and have therefore penetrated various electronic applications, such as organic photovoltaics (OPVs), organic field-effect transistors (OFETs), and organic light-emitting diodes (OLEDs). These applications have made steady progress. Particularly, high charge carrier mobility over 10 cm² V⁻¹ s⁻¹ has been achieved in OFET applications.¹ However, at a fixed device voltage, increased carrier mobility in an OFET generates a larger electrical current and Joule heating effect, leading to ineluctable thermal degradation of the device during operation. Worse, the thermal conductivity of existing OSCs, especially amorphous OSCs, is in a very low range below 1 W m⁻¹ K⁻¹ due to structural disorders and weak molecular interactions.^{2–4} This undesirable thermal conductivity is extremely unfavorable for heat dissipation in devices, but relevant studies to alleviate this problem are very lacking.

One way of circumventing the poor thermal conductivity in OSCs is a blending approach. In general, blending high thermal conductivity fillers, e.g., metal and ceramic particles, in OSC materials has been considered a desirable strategy.^{5–7} The fillers serve as the heat dissipation materials to release the heat accumulated during the device operation, thereby constructing thermally durable devices. However, this approach poses challenges for scaled-up applications due to the high material cost and the risks of degrading electrical and optical properties.^{8,9} Recently, Gumyusenge et al. found that blending insulators into OSCs was beneficial to the thermal

stability of devices, which facilitated a high-mobility operation at up to 220 °C.¹⁰ This stems from the fact that the conformational change of OSCs under heating is restricted by the insulator. However, comprehensive studies on the heat transfer effect of OSC after incorporating insulators were rarely explored; the corresponding mechanism is still unclear. Hence, it is highly desirable to systematically study the thermal properties of the blended system and disclose the role of insulators in the blends for realizing efficient heat transfer.

Here, we chose [6,6]-phenyl-C71-butyric acid methyl ester (PC₇₁BM) as the host OSC. PC₇₁BM is known to have very poor heat conduction properties in the condensed phase due to severe vibrational scattering of electrons by its molecular tail.^{11–15} Yet, it is probably the most popular electron transporter used in organic electronics. Into PC₇₁BM, we blended a small amount of one of the most easily accessible insulators, polystyrene (PS). It is found that the addition of PS can enhance the thermal stability of the as-prepared OFETs. The device reproducibility is improved while suppressing leakage current in the off-state (*I*_{off}) and subthreshold swing

Received: April 3, 2022

Accepted: June 8, 2022

Published: June 23, 2022



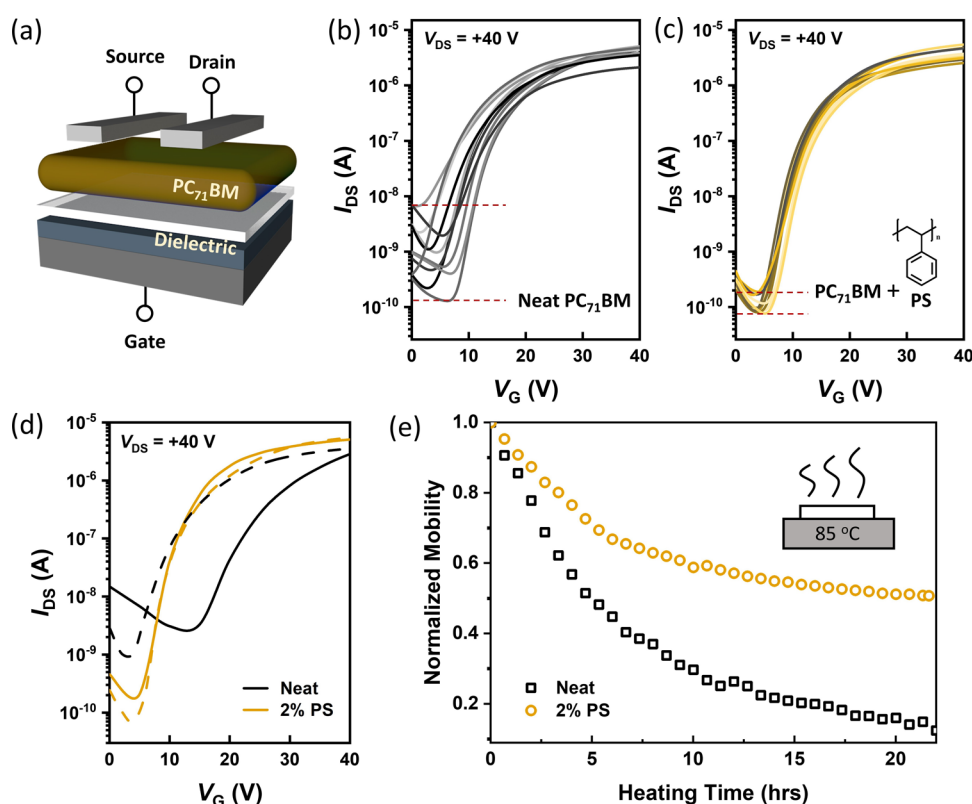


Figure 1. (a) Schematic illustration of OFET configuration. Typical transfer curves of PC₇₁BM-based OFETs (b) without and (c) with 2% PS incorporation at room temperature (each curve represents a single batch). (d) Transfer characteristics of neat PC₇₁BM and PC₇₁BM/PS-based OFETs before (dashed lines) and after heating at 85 °C (solid lines). (e) Normalized field-effect mobility as a function of heating time.

Table 1. Summary of OFET Parameters: Field-Effect Mobility, Off Current, Threshold Voltage (V_{th}), and Subthreshold Swing (SS)

sample	mobility ($\text{cm}^2 \text{V}^{-1} \text{s}^{-1}$)	off current (A)	V_{th} (V)	SS (V dec^{-1})
neat PC ₇₁ BM	$(1.2 \pm 0.2) \times 10^{-2}$	$(1.2 \pm 1.8) \times 10^{-9}$	7.9 ± 2.0	2.8 ± 1.0
PC ₇₁ BM/2% PS	$(1.4 \pm 0.2) \times 10^{-2}$	$(0.9 \pm 0.4) \times 10^{-10}$	8.8 ± 0.7	1.9 ± 0.2

(SS). The effect of insulators on heat transfer was then examined using the scanning photothermal deflection (SPD) technique and an infrared thermal imaging camera (IR camera), where the thermal diffusivity measured by SPD characterizes the rate of heat dissipation. SPD shows that the thermal diffusivity of a blended film is doubled to $1.01 \text{ mm}^2 \text{ s}^{-1}$ when compared with a neat PC₇₁BM film. Furthermore, the application of blends in electron transport layers of perovskite solar cells confirms the potential applicability of the insulator blend approach. Finally, the ternary phase diagrams comprising PS with varied molecular weights (MWs) were calculated to understand the underlying mechanism for the role of insulators in the mixtures. The better mixing of OSC and low-MW insulator allows for a more interconnected phonon transport network, thereby facilitating heat propagation. This work not only offers an understanding of heat transfer in OSC/insulator blends but also enriches the development of OSCs with promising stability for various electronic applications.

2. RESULTS AND DISCUSSION

2.1. OFET Characteristics. 2.1.1. Electrical Properties.

OFETs were first fabricated to investigate the electrical properties of neat PC₇₁BM and PC₇₁BM/PS (weight ratio of 98:2, MW of PS is 4 kDa) films using a bottom-gate top-

contact configuration (Figure 1a). Figure 1b,c shows the typical transfer characteristics of PC₇₁BM-based OFETs in different batches, without and with PS incorporation, respectively. Their corresponding output curves and the results of different PS concentrations are shown in Figure S1. When PS is added to PC₇₁BM, counterintuitively, the resultant OFETs can still sustain the field-effect mobilities (Table 1), although the electrically inert polymer was expected to impede the charge transport. Two important OFET parameters, I_{off} and SS, determine the power consumption and the speed of a transistor, closely related to the practical scenarios. However, the neat PC₇₁BM devices display relatively high I_{off} [$(1.2 \pm 1.8) \times 10^{-9} \text{ A}$] and SS ($2.8 \pm 1.0 \text{ V dec}^{-1}$) levels after counting all measured devices (Table 1). Remarkably, 2% PS added in the OFETs can narrow device-to-device parameter spread and effectively reduce I_{off} and SS to $(0.9 \pm 0.4) \times 10^{-10} \text{ A}$ and $1.9 \pm 0.2 \text{ V dec}^{-1}$, respectively. Evidently, an appropriate amount of PS in the mixture does not impair the electrical performances of PC₇₁BM-based OFETs. More interestingly, improved and more consistent OFET parameters (I_{off} and SS) can be obtained with this facile blending approach. The improvement of I_{off} and SS levels in the insulator blends was also seen in several prior investigations performed by other researchers.^{16,17} The origin of such improvement has been

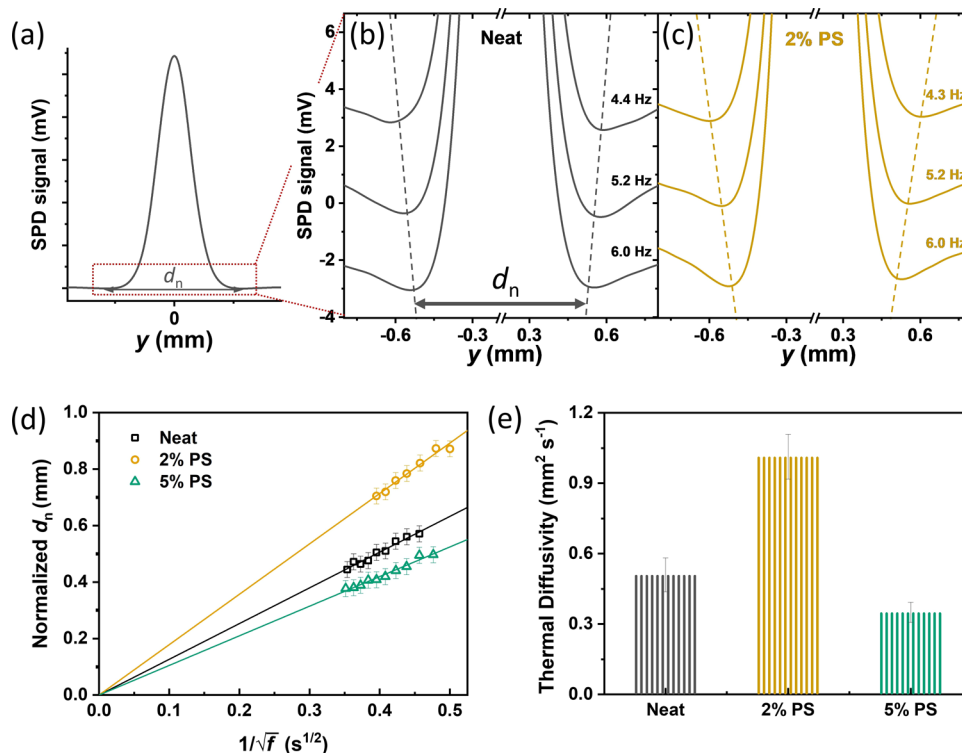


Figure 2. (a) Typical thermal wave pattern measured by the scanning photothermal deflection (SPD). The magnified SPD signals in the red rectangle of (a) at selected modulating frequencies: PC₇₁BM films (b) without and (c) with 2% PS addition. (d) Normalized d_n versus $1/\sqrt{f}$ plot. The solid lines are linear fits of eq 1. (e) Thermal diffusivities of PC₇₁BM films made using different concentrations of PS.

attributed to the smoothing and depolarization of the underlying gate dielectric layer.¹⁸

2.1.2. Thermal Stability. When the OFETs are heated at a high temperature, e.g., 85 °C, the devices may suffer performance degradation. For example, it has been reported that I_{off} in the device increases exponentially with temperature, and the correspondingly increased energy loss is detrimental to the OFETs in practical operating scenarios.¹⁹ As shown in Figure 1d, for the neat device after heating, I_{off} and threshold voltage are shifted up ($\sim 10^{-9}$ A) and to the right (~ 18 V), respectively. Conversely, such a high temperature has no significant effect on OFETs made of blends comprising 2% PS, at which their comparatively low I_{off} of $\sim 10^{-10}$ A and threshold voltage of ~ 8 V contribute to reduced power consumption in the device.

During continuous thermal stress being applied, the OFETs with PS can better maintain their field-effect mobility (Figure 1e) and source-to-drain current (Figure S2). Specifically, the devices retain more than 50% of initial mobility and an on/off ratio of $> 5 \times 10^4$ after subjecting to heating for 15 h, while the neat devices, in stark contrast, undergo a faster drop in mobility to around 20% of their initial mobility and a smaller on/off ratio of around 10^3 using the same procedure. It is possibly due to the thermally induced aggregation of PC₇₁BM.^{20–23} In addition to thermal stability, the operational stability under continuous bias stress was also studied. Compared with the neat device under high-voltage stress, the PS-added counterpart yields a higher output current (Figure S3a). The transfer curves were measured in a rapid sequence after biasing (Figure S3b). It shows that the neat PC₇₁BM-based device exhibits an abnormal transfer shape, while high-voltage stress has a less pronounced impact on the PS-added device. This result further demonstrates that the insulator

incorporation can effectively improve the heat dissipation in OSC devices, which can extend their operation lifetime. To verify the generality of heat transfer improvement with the blend approach, we employed the blends of PS with a nonfullerene small-molecule OSC, (2,2'-[[6,6,12,12-tetrakis(4-hexylphenyl)-6,12-dihydrodithieno[2,3-d:2',3'-d']-s-indaceno[1,2-b:5,6-b']dithiophene-2,8-diyl]bis[methylydene(3-oxo-1H-indene-2,1(3H)-diylidene)]]bis[propanedinitrile]) (ITIC). In ITIC/PS blended devices, similar trends with improved I_{off} reproducibility, and thermal stability relative to the neat ITIC devices can be observed in Figure S4.

2.2. Heat Transfer. **2.2.1. Thermal Diffusivity.** To explore the origins of the improved thermal stability, we used the highly sensitive scanning photothermal deflection (SPD) technique to probe the thermal diffusivity of thin films without and with PS. Thermal diffusivity quantifies how fast heat propagates or diffuses through the material. The principle of SPD is briefly described below:²⁴ the sample is immersed in a transparent deflection fluid and illuminated by a modulated monochromatic pump beam. Due to optical absorption, the sample is heated up and causes a temperature increase in the adjacent deflecting fluid, resulting in its refractive index changes. A laser probe beam launched parallel to and above the sample surface is deflected by changes in the refractive index. The deflection signal can be measured as a function of distance y between the pump beam and the probe beam. The resulting SPD signal versus y can be interpreted as a surface temperature profile (thermal wave) induced by the heating of the pump beam. Figure 2a shows a typical thermal wave pattern of the lateral temperature profile of the sample upon light illumination, i.e., the SPD signal: The signal reaches a maximum at the center of pump beam irradiation ($y = 0$). When away from the irradiation center, the surface temper-

ature decreases and reaches two minima symmetrically on both sides, with separation d_n between the minima. d_n increases with the decrease of modulated pump frequency (f) due to the longer heat diffusion time and the larger spatial temperature gradient. The magnified SPD spectra of measured samples at selected modulating frequencies are shown in Figure 2b,c, and the full SPD spectra can be found in Figure S5. Figure 2d offers the relationship between $1/\sqrt{f}$ and normalized d_n that were deduced from Figure S5. Then, thermal diffusivity D can be inferred from the slope of the plot using the following equation^{25,26}

$$D = \frac{1}{\pi} \left(\frac{\partial d_n}{\partial f^{-1/2}} \right)^2 \quad (1)$$

The extracted D for PC₇₁BM films mixed with different concentrations of PS is plotted in Figure 2e. The results show that the thermal diffusivity of the neat PC₇₁BM film at room temperature is 0.51 mm² s⁻¹ and doubles to 1.01 mm² s⁻¹ after adding 2% PS ($D_{\text{PS}} = 0.117 \text{ mm}^2 \text{ s}^{-1}$),²⁷ which is summarized in Table 2. However, the heat diffusion is inhibited when the

Table 2. Thermal Diffusivities (D) Measured by the SPD Technique^a

	D (mm ² s ⁻¹)	k (s ⁻¹)
neat PC ₇₁ BM	0.51 ± 0.07	0.15
PC ₇₁ BM/2% PS	1.01 ± 0.10	0.27
PC ₇₁ BM/5% PS	0.35 ± 0.04	

^aExponential decay parameters (k) fitted to the data (Figure 3C) measured by an infrared thermal camera.

insulator loading further increases to 5%. The enhancement of thermal diffusivity suggests a better heat transfer ability inside the blended film with an appropriate amount of PS.

2.2.2. Thermal Images. For a more intuitive demonstration of the difference in heat transfer in the insulator-added films, a cooling test was carried out (Figure 3a). Two samples without and with the insulator were heated at a temperature higher than the surrounding environment and then immediately transferred to the ambient plate (20 °C) to explore how heat is dissipated on the films over time.²⁸ The cooling process was monitored by an IR camera, by which the differences in the surface temperature of the samples were visually evident (Figure 3). The surface temperature decays rapidly during the natural cooling process, accompanied by a gradually darkening color. In the beginning, the initial temperature (0 s) of the two samples is identical. After 5 s, the PS-added sample only shows a temperature of around 33 °C, while the control one remains at a higher temperature of about 37 °C (Figure 3b). A similar trend can be observed at the other heating temperatures, with the results shown in Figure S6a. The temperature profiles of each sample can be fitted by Newton's cooling law with an exponential decay coefficient k (Figures 3c and S6b). The extracted k for the insulator-containing film ($k = 0.27 \text{ s}^{-1}$) is almost twice that of the neat film ($k = 0.15 \text{ s}^{-1}$) (Table 2). The faster cooling rate in the blended film further supports that the insulator has promoted heat dissipation in OSCs, avoided overheating during operation, and thus improved the device stability. A similar trend with ITIC demonstrates the universality of insulators in improving the thermal behaviors of OSCs (Figure S7).

2.3. PC₇₁BM/PS in ETL of Perovskite Solar Cells. The previous section offers an observation of the improved heat transfer properties of PC₇₁BM/PS blends as a solid film. This observation is general and does not depend on a specific device structure. Therefore, the film can be employed in (i) an n-channel OFET (Section 2.1) or (ii) an electron transport layer (ETL) in other electronic devices. In (ii), we select perovskite solar cells (PSCs), as they are topics of huge concern in thin-film photovoltaics, and our work also provides a new strategy

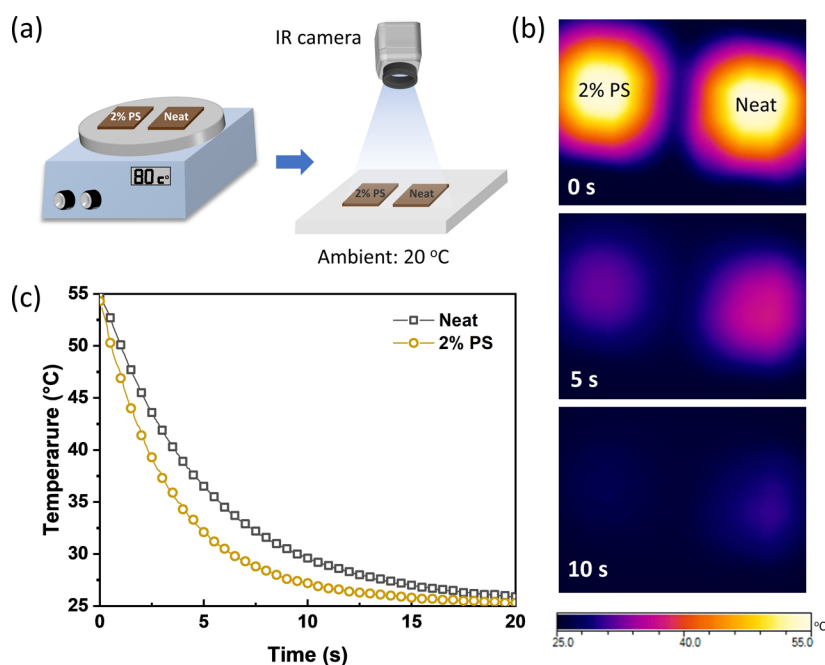


Figure 3. (a) Schematic of the cooling test using an infrared thermal imaging camera (IR camera). (b) Corresponding thermal images at the selected time. (c) Transient variations of surface temperatures based on PC₇₁BM films without and with PS incorporation.

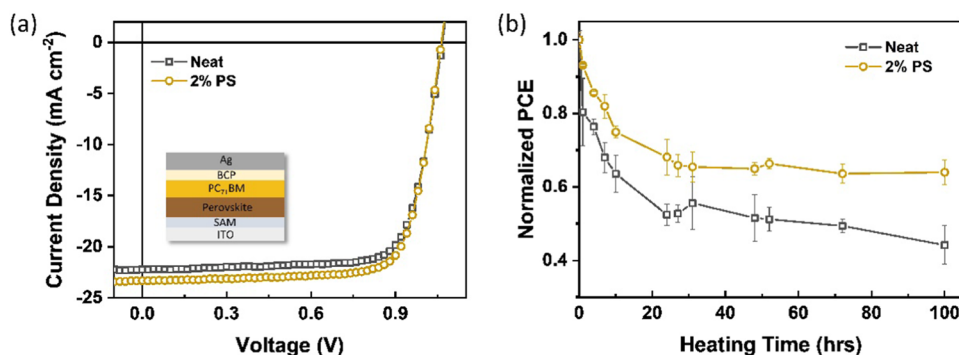


Figure 4. (a) J - V curves of typical perovskite solar cells (PSCs) without and with PS in the PC₇₁BM electron transport layer (ETL). (b) Shelf lifetime tracking of optimized PSCs under constant thermal stress (65 °C) for 100 h.

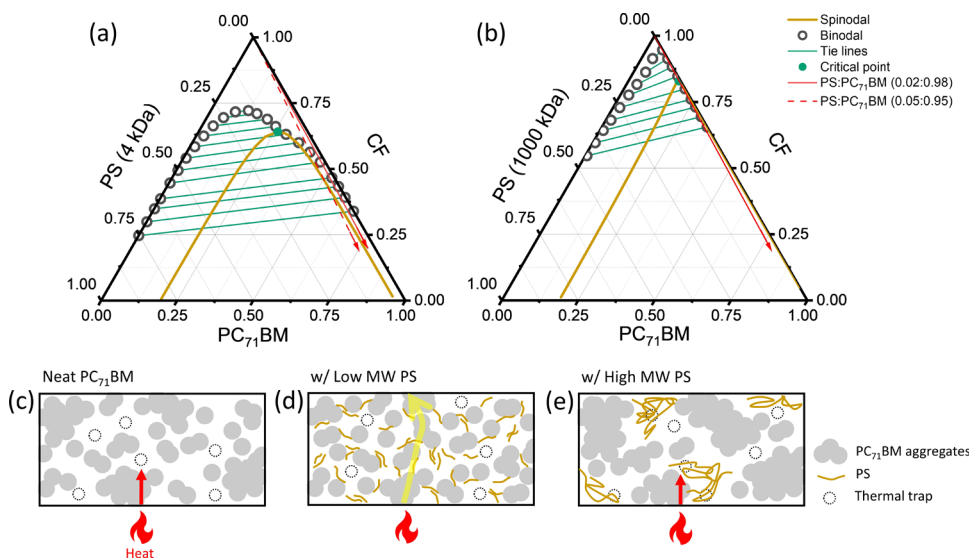


Figure 5. Phase diagrams for the ternary PC₇₁BM/PS/chloroform (CF) system with two different molecular weights (MWs) of PS: (a) MW = 4 kDa and (b) MW = 1000 kDa. The intersection of binodal and spinodal lines is the critical point. The red arrows denote the solvent quenching line with PC₇₁BM:PS weight ratios of 98:2 (solid arrow) and 95:5 (dashed arrow). (c–e) Schematic illustration of neat OSC and blended films made using two different MWs of PS.

to manage heat dissipation in these photovoltaic cells. Following this line of thought, inverted planar-structured PSCs were fabricated in which fullerene is usually used as an ETL. However, the fullerene ETL has been identified as a key origin of instability in these cells, which has to be addressed promptly, particularly for thermal stability, yet only a few studies have been conducted.²⁹ Here, we employ the PC₇₁BM/PS film as ETL in PSCs to investigate the effect of PS on the thermal stability of the PSCs. Two beneficial effects were observed. First, the as-prepared cell with the PS-added PC₇₁BM film as ETL has a slightly larger short-circuit current (J_{SC}) and fill factor (FF) and thus an improved average power conversion efficiency (PCE) of 18.34% (Figure 4a), when compared with the PSC in the absence of the insulator (17.87%). Their corresponding characteristic parameters, including PCE, open-circuit voltage (V_{OC}), J_{SC} , and FF are summarized in Table S1. Second, the long-term thermal stability of PSCs is improved. As shown in Figure 4b, the measured PCEs degrade monotonically as heating time increases. For the control devices containing the neat PC₇₁BM film, only 44% of its initial PCE remains after heating at 65 °C for 100 h. The presence of the insulator in the ETL, in contrast, better stabilizes the PCEs of the devices to resist

thermal stress. The PCE can be maintained at nearly 12%, equivalent to ~64% of its initial PCE under the same test conditions. In summary, in comparison with the neat PC₇₁BM film as ETL, photovoltaic parameters can be maintained or even slightly improved when employing the OSC/insulator blends in the PSC field. More importantly, the durability of devices against thermal stress is improved due to the efficient heat transfer in blended films. These results are in line with previous observations, indicating that the insulator-mixed fullerene films can be potentially suitable ETLs for PSCs under high-temperature working conditions.

2.4. How PS Improves Thermal Transport? **2.4.1. Morphology.** To gain insight into the improved thermal transport in the blended films, the surface morphology of PC₇₁BM and ITIC films before and after PS incorporation was investigated by atomic force microscopy (AFM) (Figures S8 and S9). The AFM images reveal that the neat PC₇₁BM film possesses a rather flat and featureless surface, consistent with previous reports.^{30–32} The surface morphology remains comparable to that of the neat film upon the addition of 2% PS, whereas the corresponding root-mean-square roughness is reduced from 0.28 to 0.19 nm. The smoother surface suggests that the incorporation of PS aids in the formation of a uniform film.³³

However, when the PS concentration is increased to 5%, distinct phase separation can be observed (Figure S8), which may explain the suppressed thermal diffusivity of PC₇₁BM at high PS loading (Figure 2e). The probed X-ray diffraction (XRD) spectra show that incorporating 2% PS does not exert a significantly observable effect on the crystallinity of the PC₇₁BM film, as shown in Figure S10a. Together with similar absorption spectra of the neat and PS-added films (Figure S10c), it is noticeable that the surface morphology and crystalline packing of OSC films are quite insensitive to 2% PS inclusion.

2.4.2. Chain Length Effect. It has been reported that the molecular weight (MW) (or the chain length) of the insulating polymer has a substantial impact on the device performances of OSC/insulator blends.^{17,34,35} To investigate the MW effect, we used another high-MW PS, 1000 kDa PS, to fabricate blended OFETs, as shown in Figure S11a. Unlike previous blends with lower MW 4 kDa of PS, the I_{off} of the devices blended with 1000 kDa PS undergoes an upward shift, even higher than the neat PC₇₁BM device. In addition to the inferior OFET performance, the high-MW-based blends yield slower heat dissipation when directly compared with the neat film (Figure S11b). These findings indicate that the electrical and thermal behaviors of the blends strongly depend on the MW of PS.

To further explore the underlying mechanism and understand the phase behaviors of components in the blended system, the ternary phase diagrams consisting of PS, PC₇₁BM, and solvent components were calculated based on Flory–Huggins theory, as shown in Figure 5a,b (the calculation parameters can be found in Tables S2 and S3 and the details are discussed in the Supporting Information). The single-phase and phase-separated regions are distinguished by the binodal line, i.e., the miscibility boundary, which is determined by the chemical potential equilibrium of liquid phases. The spinodal line and critical point are derived from the second and third derivatives of Gibbs free energy, respectively. Spinodal decomposition takes place in the region below the spinodal, where liquid–liquid (L–L) phase separation occurs spontaneously due to the repulsive interaction between PS and PC₇₁BM molecules. Tie lines represented by green lines connect the binodal compositions with equal chemical potentials.

Figure 5a,b shows that adding a certain amount of PS with different MWs has significantly diverse effects on the ternary phase diagram. In the low-MW-based system (Figure 5a), a small miscibility gap, denoted as open dots, indicates a low probability of presolidification phase separation and favorable miscibility.³⁶ In the presence of a high-MW polymer (Figure 5b), the miscibility gap expands and almost covers the entire diagram. The asymmetry of binodal is due to the large size difference between PC₇₁BM and high-MW polymer.³⁷ Obviously, the ternary system composed of high-MW PS is less miscible than the one containing low-MW PS. The red arrows in Figure 5a,b are the solvent quenching lines that indicate the changes in the overall composition of the mixed solution upon solvent evaporation,³⁸ in which the solid arrows represent the subsequent continuous evaporation of the PC₇₁BM:PS mixture with a weight ratio of 98:2. Upon further increasing PS concentration to 5%, the solvent quenching line (red dashed arrow) in the ternary phase diagram will directly enter the thermodynamically unstable region below the spinodal (yellow line), where L–L demixing is present, as

already hinted by AFM results (Figure S8d). The same goes for the solvent quenching line in the case of high-MW-based blends with a PC₇₁BM:PS weight ratio of 98:2 (Figure 5b), in which solvent evaporation drives the system into the unstable part of the phase diagram, triggering the separation of PC₇₁BM and high-MW PS phases.

Based on the phase analysis, Figure 5c–e offers a model to explain the effect of the PS chain length on the heat transfer of blends. In the neat PC₇₁BM film (Figure 5c), the predominantly isolated PC₇₁BM domains are formed due to the highly localized vibrations, resulting in poor heat conduction.¹² In addition, the fullerene aggregation under thermal stress worsens the situation. When low-MW PS is added to PC₇₁BM, the intimacy of mixing demonstrated by a small miscibility gap means that more low-MW polymers are prone to distribute in the PC₇₁BM domains, hindering the growth of PC₇₁BM aggregates, consequently allowing the formation of interconnected phonon transport network, in which PS can bridge effective conductive regions providing “highways” for phonon propagation due to the efficient phonon transport of PS chains (Figure 5d).^{39,40} When the high-MW PS is blended with PC₇₁BM, the mixtures tend to separate into individual phases due to the repulsive interaction between OSC and PS. In this two-phase structure, PS phases are too “pure” and scatter phonons as impurities, disrupting the percolation pathways, thus hampering the phonon transport in the blended film (Figure 5e). Therefore, PS needs to be well mixed with OSC and avoid two-phase demixing to achieve efficient phonon propagation in the blends.

3. CONCLUSIONS

This work studies the effect of PS on the thermal performances of OSCs, even though PS is generally considered to be electrically and thermally insulating. The addition of PS can effectively boost the heat transfer of OSCs, which can be reflected by the improved thermal stability in OFET and PSC configurations, the increased thermal diffusivity in the SPD technique, and the enhanced heat dissipation indicated by an IR camera. These improvements are achieved without sacrificing electrical properties. The computed ternary phase diagrams suggest that the low-MW PS is intimately mixed with OSC, which enables efficient phonon transport by forming percolated PC₇₁BM/PS phonon pathways. In contrast, the separation between the high-MW insulator and OSC phases in the blends leads to poor heat conduction. The insulator blend approach provides a facile path for diverse thermal management and thermal-based applications by tuning the thermal properties of OSCs.

4. EXPERIMENTAL SECTION

4.1. Materials and Thin-Film Fabrication. PC₇₁BM, PS, and ITIC were purchased from Nano-C, Polymer Source, and 1-Material Inc., respectively. All of the materials were used as received without further purification. The OSC solution has a concentration of 10 mg mL⁻¹ in anhydrous chloroform (Sigma Aldrich). PS with the same concentration was separately prepared and stirred in a glovebox overnight before using. Then, the PS solution was added to the OSC solution directly at various compositions to form different blended OSC/PS solutions. The active layer was spin-coated at a speed of 1400 rpm for 30 s using these solutions in a nitrogen-filled glovebox.

4.2. Device Fabrication. **4.2.1. OFET Fabrication.** The Si/SiO₂ wafers were subjected to ultrasonication and rinsed with deionized water, acetone, and 2-propanol for 20 min each, followed by drying

with compressed air. After being treated with an ultraviolet–ozone cleaner (Jelight, UVO cleaner, Model 42–220) for 13 min, the substrates were transferred to a glovebox for spin coating. Poly-(2,3,4,5,6-pentafluorostyrene) (PPFS) dissolved in methyl isobutyl ketone with a concentration of 10 mg/mL was spin-coated at 2000 rpm for 60 s as the gate dielectric layer.⁴¹ The active layers were spin-coated on the top of the PPFS film without further annealing. Finally, LiF/Al (1 nm/100 nm) electrodes were coated on the samples in a high vacuum chamber ($\sim 4 \times 10^{-6}$ Torr) through a shadow mask, defining a 50 μm channel length.

4.2.2. PSC Fabrication. The Indium tin oxide (ITO) patterned substrates were cleaned prior to the device fabrication by sonication in deionized water, acetone, and 2-propanol, respectively. The self-assembled monolayer molecule ([2-(3,6-dimethoxy-9H-carbazol-9-yl)ethyl]phosphonic acid) (MeO-2PACz) was spin-coated on the substrates. Then, the perovskite film ($\text{CH}_3\text{NH}_3\text{PbI}_3$) was spin-coated with the typical one-step solution method.⁴² After that, PC_{71}BM or $\text{PC}_{71}\text{BM}/\text{PS}$ film and bathocuproine (BCP) film were deposited on the active layer, respectively. Finally, 80 nm of Ag was evaporated on the top of films and served as the cathodes in a high vacuum chamber.

4.3. Characterization. All OFET measurements were taken in a cryostat (Oxford Instruments, Optistat DN-V) under vacuum (below 10^{-4} Torr) and dark conditions. During OFET measurements, a Keithley 236 source measurement unit was used to provide the source-to-drain bias, while a Xantrex XT 120-0.5 was used to supply the gate voltage. The field-effect mobilities were extracted from the saturation regime of transfer curves. In SPD measurement, the samples were immersed into perfluorohexane as the deflection fluid and irradiated by a 5 mW, 532 nm laser diode as the pump beam. The pump beam was modulated by a mechanical chopper with specific frequencies and focused by a convex lens. The deflection of a probe beam (2 mW 632 nm He–Ne laser) on the sample surface due to the released heat was detected by a silicon PIN photoquadrant detector (TEMic). A position sensor, together with a chopper, was connected to the Stanford Research SR830 lock-in amplifier to collect the data. The thermal images were taken by an IR camera (Optris PI 400i). The surface morphology of the thin films was probed by an atomic force microscope (AFM) (Veeco Deltak 150 surface profiler) operating in tapping mode.

■ ASSOCIATED CONTENT

Supporting Information

The Supporting Information is available free of charge at <https://pubs.acs.org/doi/10.1021/acsami.2c05503>.

OFET output characteristics, thermal and bias stress test, OFET characteristics of the ITIC system, SPD signals, transient variations of surface temperature, photovoltaic parameters of perovskite solar cells, AFM topography, XRD spectra, optical absorption spectra, and computational details about the ternary phase diagrams (PDF)

■ AUTHOR INFORMATION

Corresponding Authors

Chun Cheng – Department of Materials Science and Engineering, Southern University of Science and Technology, Shenzhen 518055, P. R. China; orcid.org/0000-0001-5976-3457; Email: chengc@sustech.edu.cn

Shu Kong So – Department of Physics and Institute of Advanced Materials, Hong Kong Baptist University, Kowloon Tong, Hong Kong SAR 999077, P. R. China; Email: skso@hkbu.edu.hk

Authors

Zhuoqiong Zhang – Department of Physics and Institute of Advanced Materials, Hong Kong Baptist University, Kowloon

Tong, Hong Kong SAR 999077, P. R. China; Department of Materials Science and Engineering, Southern University of Science and Technology, Shenzhen 518055, P. R. China;

orcid.org/0000-0003-3121-9948

Yabing Tang – State Key Laboratory for Mechanical Behavior of Materials, Xi'an Jiaotong University, Xi'an 710049, P. R. China

Yunfan Wang – Department of Materials Science and Engineering, City University of Hong Kong, Kowloon Tong, Hong Kong SAR 999077, P. R. China

Zixin Zeng – Department of Materials Science and Engineering, City University of Hong Kong, Kowloon Tong, Hong Kong SAR 999077, P. R. China

Run Shi – Department of Materials Science and Engineering, Southern University of Science and Technology, Shenzhen 518055, P. R. China; orcid.org/0000-0002-3214-4661

Han Yan – State Key Laboratory for Mechanical Behavior of Materials, Xi'an Jiaotong University, Xi'an 710049, P. R. China; orcid.org/0000-0002-9693-7695

Sai-Wing Tsang – Department of Materials Science and Engineering, City University of Hong Kong, Kowloon Tong, Hong Kong SAR 999077, P. R. China

Complete contact information is available at:

<https://pubs.acs.org/doi/10.1021/acsami.2c05503>

Author Contributions

The manuscript was written through the contribution of all authors. All authors have given approval to the final version of the manuscript.

Notes

The authors declare no competing financial interest.

■ ACKNOWLEDGMENTS

Support to this work by the Research Grant Council of Hong Kong under Grant # HKBU12200119 is gratefully acknowledged. The authors also acknowledge the support from the National Natural Science Foundation of China (Grant no. 91963129) and the Basic Research Project of Science and Technology Plan of Shenzhen (Grant no. JCYJ20180504165655180).

■ REFERENCES

- (1) Hu, P.; He, X.; Jiang, H. Greater than 10 $\text{Cm}^2 \text{V}^{-1} \text{S}^{-1}$: A Breakthrough of Organic Semiconductors for Field-Effect Transistors. *InfoMat* **2021**, *3*, 613–630.
- (2) Mehra, N.; Mu, L.; Ji, T.; Yang, X.; Kong, J.; Gu, J.; Zhu, J. Thermal Transport in Polymeric Materials and across Composite Interfaces. *Appl. Mater. Today* **2018**, *12*, 92–130.
- (3) Xu, X.; Zhou, J.; Chen, J. Thermal Transport in Conductive Polymer-Based Materials. *Adv. Funct. Mater.* **2020**, *30*, No. 1904704.
- (4) Kim, N.; Domercq, B.; Yoo, S.; Christensen, A.; Kippelen, B.; Graham, S. Thermal Transport Properties of Thin Films of Small Molecule Organic Semiconductors. *Appl. Phys. Lett.* **2005**, *87*, No. 241908.
- (5) Wang, X.; Parrish, K. D.; Malen, J. A.; Chan, P. K. L. Modifying the Thermal Conductivity of Small Molecule Organic Semiconductor Thin Films with Metal Nanoparticles. *Sci. Rep.* **2015**, *5*, No. 16095.
- (6) Huang, C.; Qian, X.; Yang, R. Thermal Conductivity of Polymers and Polymer Nanocomposites. *Mater. Sci. Eng., R* **2018**, *132*, 1–22.
- (7) Pei, F.; Li, N.; Chen, Y.; Niu, X.; Zhang, Y.; Guo, Z.; Huang, Z.; Zai, H.; Liu, G.; Zhang, Y.; Bai, Y.; Zhang, X.; Zhu, C.; Chen, Q.; Li, Y.; Zhou, H. Thermal Management Enables More Efficient and Stable Perovskite Solar Cells. *ACS Energy Lett.* **2021**, *6*, 3029–3036.

- (8) Chen, H.; Ginzburg, V. V.; Yang, J.; Yang, Y.; Liu, W.; Huang, Y.; Du, L.; Chen, B. Thermal Conductivity of Polymer-Based Composites: Fundamentals and Applications. *Prog. Polym. Sci.* **2016**, *59*, 41–85.
- (9) Kim, G.-H.; Lee, D.; Shanker, A.; Shao, L.; Kwon, M. S.; Gidley, D.; Kim, J.; Pipe, K. P. High Thermal Conductivity in Amorphous Polymer Blends by Engineered Interchain Interactions. *Nat. Mater.* **2015**, *14*, 295–300.
- (10) Gumyusenge, A.; Tran, D. T.; Luo, X.; Pitch, G. M.; Zhao, Y.; Jenkins, K. A.; Dunn, T. J.; Ayzner, A. L.; Savoie, B. M.; Mei, J. Semiconducting Polymer Blends That Exhibit Stable Charge Transport at High Temperatures. *Science* **2018**, *362*, 1131–1134.
- (11) Duda, J. C.; Hopkins, P. E.; Shen, Y.; Gupta, M. C. Exceptionally Low Thermal Conductivities of Films of the Fullerene Derivative PCBM. *Phys. Rev. Lett.* **2013**, *110*, No. 015902.
- (12) Giri, A.; Chou, S. S.; Drury, D. E.; Tomko, K. Q.; Olson, D.; Gaskins, J. T.; Kaehr, B.; Hopkins, P. E. Molecular Tail Chemistry Controls Thermal Transport in Fullerene Films. *Phys. Rev. Mater.* **2020**, *4*, No. 065404.
- (13) Olson, J. R.; Topp, K. A.; Pohl, R. O. Specific Heat and Thermal Conductivity of Solid Fullerenes. *Science* **1993**, *259*, 1145–1148.
- (14) Giri, A.; Hopkins, P. E. Spectral Contributions to the Thermal Conductivity of C₆₀ and the Fullerene Derivative PCBM. *J. Phys. Chem. Lett.* **2017**, *8*, 2153–2157.
- (15) Pöhls, J.-H.; Johnson, M. B.; White, M. A. Origins of Ultralow Thermal Conductivity in Bulk [6,6]-Phenyl-C₆₁-Butyric Acid Methyl Ester (PCBM). *Phys. Chem. Chem. Phys.* **2016**, *18*, 1185–1190.
- (16) Cheng, H.-L.; Lin, J.-W.; Ruan, J.; Lin, C.-H.; Wu, F.-C.; Chou, W.-Y.; Chen, C.-H.; Chang, C.-K.; Sheu, H.-S. Spontaneous Formation of an Ideal-Like Field-Effect Channel for Decay-Free Polymeric Thin-Film Transistors by Multiple-Scale Phase Separation. *ACS Appl. Mater. Interfaces* **2015**, *7*, 16486–16494.
- (17) Niazi, M. R.; Li, R.; Qiang Li, E.; Kirmani, A. R.; Abdelsamie, M.; Wang, Q.; Pan, W.; Payne, M. M.; Anthony, J. E.; Smilgies, D.-M.; Thoroddsen, S. T.; Giannelis, E. P.; Amassian, A. Solution-Printed Organic Semiconductor Blends Exhibiting Transport Properties on Par with Single Crystals. *Nat. Commun.* **2015**, *6*, No. 8598.
- (18) Georgakopoulos, S.; Pozo, F. G.; del Mas-Torrent, M. Flexible Organic Transistors Based on a Solution-Sheared PVDF Insulator. *J. Mater. Chem. C* **2015**, *3*, 12199–12202.
- (19) Kobayashi, K.; Murai, H.; Hayama, M.; Yamazaki, T. The Application of Hydrogenation to Amorphous Silicon Thin Film Transistors for the Decrease of the off Current. *MRS Proc.* **1991**, *219*, No. 321.
- (20) Larson, B. W.; Whitaker, J. B.; Popov, A. A.; Kopidakis, N.; Rumbles, G.; Boltalina, O. V.; Strauss, S. H. Thermal [6,6] → [6,6] Isomerization and Decomposition of PCBM (Phenyl-C₆₁-Butyric Acid Methyl Ester). *Chem. Mater.* **2014**, *26*, 2361–2367.
- (21) Hsieh, Y.-J.; Huang, Y.-C.; Liu, W.-S.; Su, Y.-A.; Tsao, C.-S.; Rwei, S.-P.; Wang, L. Insights into the Morphological Instability of Bulk Heterojunction PTB7-Th/PCBM Solar Cells upon High-Temperature Aging. *ACS Appl. Mater. Interfaces* **2017**, *9*, 14808–14816.
- (22) Yang, X.; Niu, M.; Bi, P.; Chen, Z.; Liu, J.; Hao, X. Suppressing Thermally Induced Fullerene Aggregation in Organic Solar Cells by Employing Plastic Network. *J. Phys. Chem. C* **2018**, *122*, 9843–9851.
- (23) Zheng, L.; Liu, J.; Ding, Y.; Han, Y. Morphology Evolution and Structural Transformation of Solution-Processed Methanofullerene Thin Film under Thermal Annealing. *J. Phys. Chem. B* **2011**, *115*, 8071–8077.
- (24) Chiu, K. L.; Ho, J. K. W.; Zhang, C.; Cheung, S. H.; Yin, H.; Chan, M. H.; So, S. K. Heat Transfer in Photovoltaic Polymers and Bulk-Heterojunctions Investigated by Scanning Photothermal Deflection Technique. *Nano Sel.* **2021**, *2*, 768–778.
- (25) Zhang, Z.; Ho, J. K. W.; Zhang, C.; Yin, H.; Wen, Z.; Cai, G.; Zhao, R.; Shi, R.; Lu, X.; Liu, J.; Hao, X.; Cheng, C.; So, S. K. Boosting Charge and Thermal Transport – Role of Insulators in Stable and Efficient n-Type Polymer Transistors. *J. Mater. Chem. C* **2021**, *9*, 12281–12290.
- (26) Zhang, C.; Yuan, J.; Ho, J. K. W.; Song, J.; Zhong, H.; Xiao, Y.; Liu, W.; Lu, X.; Zou, Y.; So, S. K. Correlating the Molecular Structure of A-DA'D-A Type Non-Fullerene Acceptors to Its Heat Transfer and Charge Transport Properties in Organic Solar Cells. *Adv. Funct. Mater.* **2021**, *31*, No. 2101627.
- (27) Juangsa, F. B.; Muroya, Y.; Ryu, M.; Morikawa, J.; Nozaki, T. Thermal Conductivity of Silicon Nanocrystals and Polystyrene Nanocomposite Thin Films. *J. Phys. D: Appl. Phys.* **2016**, *49*, No. 365303.
- (28) Choi, K.; Lee, J.; Choi, H.; Kim, G.-W.; Kim, H. I.; Park, T. Heat Dissipation Effects on the Stability of Planar Perovskite Solar Cells. *Energy Environ. Sci.* **2020**, *13*, 5059–5067.
- (29) Li, S.-H.; Xing, Z.; Wu, B.-S.; Chen, Z.-C.; Yao, Y.-R.; Tian, H.-R.; Li, M.-F.; Yun, D.-Q.; Deng, L.-L.; Xie, S.-Y.; Huang, R.-B.; Zheng, L.-S. Hybrid Fullerene-Based Electron Transport Layers Improving the Thermal Stability of Perovskite Solar Cells. *ACS Appl. Mater. Interfaces* **2020**, *12*, 20733–20740.
- (30) Park, Y. J.; Cha, M. J.; Yoon, Y. J.; Cho, S.; Kim, J. Y.; Seo, J. H.; Walker, B. Improved Performance in N-Type Organic Field-Effect Transistors via Polyelectrolyte-Mediated Interfacial Doping. *Adv. Electron. Mater.* **2017**, *3*, No. 1700184.
- (31) Rossbauer, S.; Müller, C.; Anthopoulos, T. D. Comparative Study of the N-Type Doping Efficiency in Solution-Processed Fullerenes and Fullerene Derivatives. *Adv. Funct. Mater.* **2014**, *24*, 7116–7124.
- (32) Chen, F.-C.; Tsai, T.-H.; Chien, S.-C. Simple Source/Drain Contact Structure for Solution-Processed n-Channel Fullerene Thin-Film Transistors. *Org. Electron.* **2012**, *13*, 599–603.
- (33) Bai, Y.; Yu, H.; Zhu, Z.; Jiang, K.; Zhang, T.; Zhao, N.; Yang, S.; Yan, H. High Performance Inverted Structure Perovskite Solar Cells Based on a PCBM:Polystyrene Blend Electron Transport Layer. *J. Mater. Chem. A* **2015**, *3*, 9098–9102.
- (34) Haase, K.; Teixeira da Rocha, C.; Hauenstein, C.; Zheng, Y.; Hamsch, M.; Mannsfeld, S. C. B. High-Mobility, Solution-Processed Organic Field-Effect Transistors from C8-BTBT:Polystyrene Blends. *Adv. Electron. Mater.* **2018**, *4*, No. 1800076.
- (35) Zhang, Z.; Shi, R.; Amini, A.; So, S. K.; Cheng, C. Organic Semiconductor–Insulator Blends for Organic Field-Effect Transistors. *Phys. Status Solidi RRL* **2022**, *16*, No. 2100602.
- (36) Kunz, A.; Blom, P. W. M.; Michels, J. J. Charge Carrier Trapping Controlled by Polymer Blend Phase Dynamics. *J. Mater. Chem. C* **2017**, *5*, 3042–3048.
- (37) Kouijzer, S.; Michels, J. J.; van den Berg, M.; Gevaerts, V. S.; Turbiez, M.; Wienk, M. M.; Janssen, R. A. J. Predicting Morphologies of Solution Processed Polymer:Fullerene Blends. *J. Am. Chem. Soc.* **2013**, *135*, 12057–12067.
- (38) Tang, Y.; Lin, B.; Zhao, H.; Li, T.; Ma, W.; Yan, H. Significance of Dopant/Component Miscibility to Efficient N-Doping in Polymer Solar Cells. *ACS Appl. Mater. Interfaces* **2020**, *12*, 13021–13028.
- (39) Shen, S.; Henry, A.; Tong, J.; Zheng, R.; Chen, G. Polyethylene Nanofibres with Very High Thermal Conductivities. *Nat. Nanotech.* **2010**, *5*, 251–255.
- (40) Nysten, B.; Gonry, P.; Issi, J.-P. Intra-and Interchain Thermal Conduction in Polymers. *Synth. Met.* **1995**, *69*, 67–68.
- (41) Ngai, J. H. L.; Chan, C. C. M.; Ho, C. H. Y.; Ho, J. K. W.; Cheung, S. H.; Yin, H.; So, S. K. A Facile and Robust Approach to Prepare Fluorinated Polymer Dielectrics for Probing the Intrinsic Transport Behavior of Organic Semiconductors. *Mater. Adv.* **2020**, *1*, 891–898.
- (42) Li, M.; Xu, X.; Xie, Y.; Li, H.-W.; Ma, Y.; Cheng, Y.; Tsang, S.-W. Improving the Conductivity of Sol–Gel Derived NiOx with a Mixed Oxide Composite to Realize over 80% Fill Factor in Inverted Planar Perovskite Solar Cells. *J. Mater. Chem. A* **2019**, *7*, 9578–9586.